The Transactions of the Korean Institute of Electrical Engineers Vol. 61, No. 5, pp. 690~697, 2012
http://dx.doi.org/10.5370/KIEE.2012.61.5.690

8/10 베어링리스 SRM의 고속 직접전류제어

High Speed Direct Current Control for the 8/10 Bearingless SRM

관 충 우* · 안 진 우†
(Zhongyu Guan · Jin-Woo Ahn)

Abstract - Novel 8/10 bearingless switched reluctance motor, which can control rotor radial positions with magnetic force, is proposed. The motor has combined characteristics of switched reluctance motor and magnetic bearing. This paper proposes a air-gap control system method of suspending force control in a bearingless switched reluctance motor (BLSRM). The proposed radial force control scheme is independent to the torque winding current. A PI direct current control (DCC) controller and look-up table are used to maintain a constant rotor air-gap. From the analysis and the experimental results, it is shown that the proposed strategy is effective in realizing a naturally decoupled radial force control of BLSRM.

Key Words : Bearingless, Switched reluctance motor, High Speed, direct current control, Radial force control

1. INTRODUCTION

Modern industrial field such as high speed machine tool, molecular pump, centrifugal pump, compressor and aerospace need high or ultra-high speed machine [1]. Many problems will happen, when traditional mechanical bearing is taken to bear the shaft of high speed or ultra-high speed machine. For example, the mechanical bearing can cause increasing of frictional drag, thermal problem and will be heavy wear in high-speed motor, which not only leads to reduce efficiency of machine and decreases service life of bearings, but also increases burden of maintenance for machine. In addition, lubrication oil cannot be used in high vacuum, ultra high and low temperature atmospheres [2-3].

In order to solve the above problems caused by conventional mechanical bearing, non-mechanical bearing techniques, such as air bearing, liquid bearing and magnetic bearing are paid more attention. They are good candidates for high speed machines. The switched reluctance motor (SRM) is a double salient and single excited motor, in which simple concentric windings are on the stator and no windings or permanent magnets are on the rotor. These mechanical structures make SRM have many advantageous characteristics such as fault tolerance, robustness, low cost and possible operation in applications of harsh environments or high temperature or high speed [4].

In the other report, one method for bearingless SRM with 8/6 type was proposed [6], in which many numbers of switches and reverse torque are hard to avoid which restrict increasing of rotor speed. At the same time, one hybrid rotor structure, called Morrison rotor, was presented [4]. In this structure, critical speed of rotor is reduced due to increasing in axial length. A bearingless SRM (BLSRM) with hybrid stator poles is proposed [5]. The benefit of this motor is that, the torque poles and the radial force poles are decoupled each other. In this paper, the speed control and direct current control (DCC) for the proposed bearingless SRM is researched.

2. STRUCTURE AND OPERATING PRINCIPLE

2.1 Review of Previous Bearingless SRM

Fig. 1(a) shows only the A-phase stator winding of a 3-phase system with additional differential windings[9]. The motor winding, N_{ma} consists of four coils connected in series. On the other hand, the suspension windings, N_{sa_1} and N_{sa_2} consist of two coils. Fig. 1(b) shows the principle of suspension force generation. The figure shows the symmetrical four-pole flux produced by the four-pole motor winding current i_{ma}, and the symmetrical two-pole flux produced by the two-pole suspension winding current i_{sa_1}. In this situation, the flux density in air-gap section 1 is increased because the direction of the two-pole flux is the same as that of the four-pole flux. In contrast, the flux density in air-gap section 2 is decreased. Therefore, superposition of the air-gap

* 준 회 원 : 경성대 메카트로닉스공학과 석사과정
† 교신저자, 펠로우회원 : 경성대 메카트로닉스공학과 교수
E-mail : jwahn@ks.ac.kr
접수일자 : 2011년 12월 15일
최종완료 : 2012년 2월 21일

magnetic flux waves results in a suspension force F acting along the x-axis. And a suspension force can be generated in any desired direction by a vector sum of these forces.

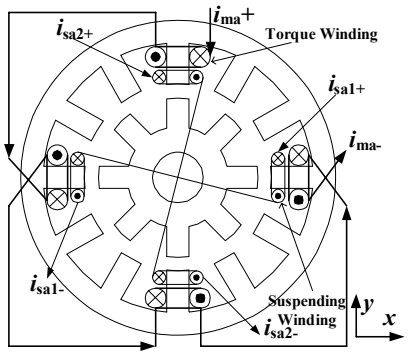

(a) A-phase winding configuration

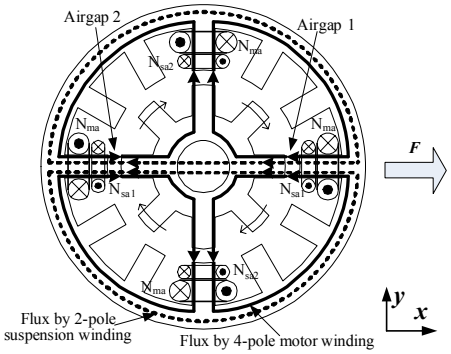

(b) Principle of suspension force generation

Fig. 1 12/8 BLSRM with differential windings

2.2 Proposed 8/10 bearingless SRM

A 8/10 bearingless SRM with separated torque and radial force winding is proposed as shown in Fig. 2. [5] Different from conventional structure, two types of stator poles are included on the stator. One is torque pole such as A_1, A_2, B_1 and B_2, which mainly produce rotational torque. The other is radial force pole such as P_{x1}, P_{x2}, P_{x3} and P_{x4}, which mainly generate radial force to suspend rotor and shaft. At the same time, pole arc of radial force is selected not to be less than one pole pitch of rotor for producing continuous radial force. Windings on the pole A_1 and pole A_2 are connected in series to construct torque winding A, and windings on the pole B_1 and pole B_2 are connected in series to construct torque winding B. Windings on poles P_{x1}, P_{x2}, P_{x3} and P_{x4}, are independently controlled to construct four radial force windings P_1, P_2, P_3 and P_4 in x- and y-directions.

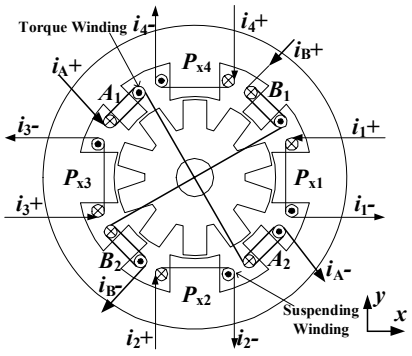

Fig. 2 Basic structure of proposed bearingless SRM

2.3 Profile of 8/10 bearingless SRM

Fig. 3 shows the characteristic curves about hybrid pole bearingless SRM.

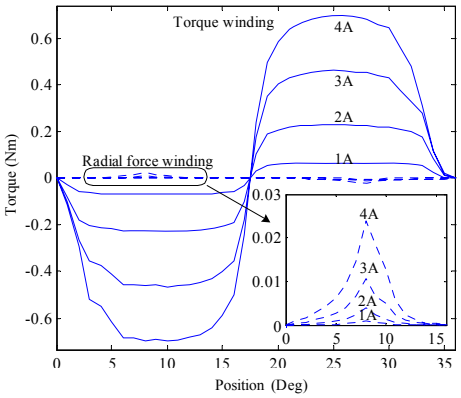

(a) Torque profiles

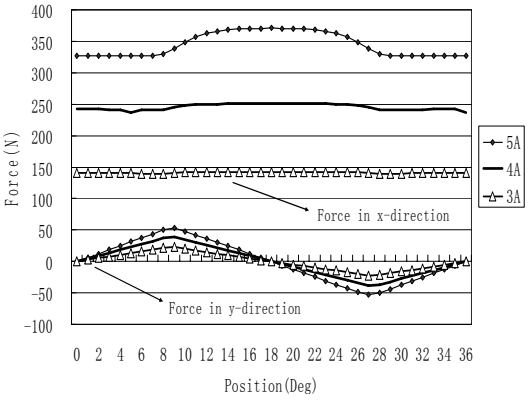

(b) Radial force profiles

Fig. 3 Analysis of hybrid pole BLSRM

Fig. 3(a) shows the torque profiles for torque and radial force winding with various rotor positions and currents. It can be seen that torque characteristic of

radial force winding changes very small for every rotor positions with the same phase current. And the torque profile of torque winding changes obviously with the variation of rotor position. Therefore, torque control can be decoupled from the radial force control. From Fig. 3(b), radial force almost can be kept constant at any position with the same excitation current. So, a large and wide radial force can be obtained only by small excitation current. But this structure also has some disadvantages. First, there are only two phase windings for generating the torque. The torque ripple is larger than that of general SRM. Second, half of stator poles is used for producing the suspending forces, the output torque is smaller than that of general SRM. Fig. 3(b) shows the radial force of the proposed motor. From the figure, the radial force can be generated proportional to the current from 3A to 4A (rated current). But in the y-axis there is another disturbed radial force in the other direction which called concomitant magnetic force. And with the different current and different position there is a different concomitant magnetic force. The concomitant magnetic force with the different eccentric rotor position is not same. Because of the eccentric displacement of the rotor, there is not much relationship between radial force and eccentric force. So, it is difficult to control the radial force by a formula.

2.4 Control principle of the radial force

Fig. 4 shows the control principle of suspending force. From this figure, when rotor has eccentric displacement in positive y- and x-direction, only current i_2 and current i_3 will be turned on and other radial force windings on the poles of and P_{x4} and P_{x1} are turned off. Accordingly, radial force in negative y- and x-direction is generated. Current i_2 and current i_3 can be regulated until rotor is in the balanced position. Using the same method, if rotor has eccentric displacement in negative x-and y-direction at the same time, only winding P_{x1} and P_{x4} need to be turned on and current i_1 and i_4 are regulated to make rotor return to its zero position. In Fig. 4, (0,0) is the center position of the motor, and (x_k,y_k) is the eccentric position of the motor. "Δx, Δy" presents the redial force generated in the x- and y-axis. And the "k_{xk},k_{yk}"is the displacement error which has the relationship with the eccentric position with the coefficient k. The white block in Fig 4 is the air gap sensor which was used for detecting the air gap. And the air gap sensor is the eddy sensor with the measuring range from 0 to 1 mm, and the output range is from 0 to 16 volt which was divided by 1 mm. For all of these parameters the radial force can be calculated by the formula of the radial force with the resolution is 0.12 μm.

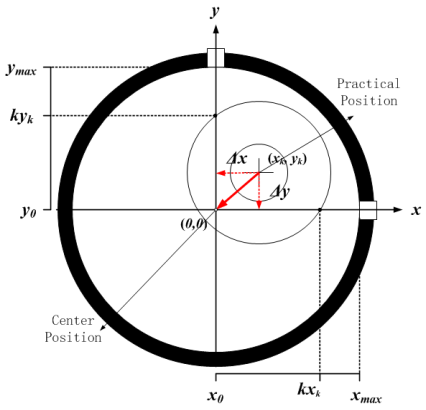

Fig. 4 Radial force control principle

3. CONTROL METHOD AND RADIAL FORCE CONTROL

3.1 Control method

In the Fig. 3(b) the x-axis shows the varying position of 36 degrees of a cycle, and y-axis is the radial force generated in the motor. The triangle line shows the radial force generated in the x-axis with 3A current, the straight and dot line show the radial force generated in the x-axis with 4A and 5A current respectively. The top three lines are the radial force generated in the main winding; the three lines in the bottom show the in the y-axis. For example, when the x-axis generates a radial force, there is another force effect on the y-axis just like the bottom curve shows in the Fig. 5, so as to the other axis. The radial force was effected by this seriously. So it is difficult to control the radial force very well with so much concomitant magnetic force. The air gap will be ununiform, afterwards there is a big effect on the torque. Then a big torque ripple will be generated, and the torque performance will be not good. The direct effect is that there will be a great noise. At the same time there will be a lot of attrition and other losses which can destroy the motor. Fig. 5 shows the radial force in the y-direction and the eccentric force in the x-axis, these two forces are all generated by the same pole.

So, in order to solve the problem, a new compensation method is proposed. As we know from the radial force curve, there are no relationship with the radial force in the other axis, so a lookup table method was used to offset the concomitant magnetic force. Just like the picture showed in the Fig. 5. The picture shows the conventional force in the x-axis, and also shows the compensation force in the same axis. The dotted line in the picture shows the compensation force which the motor needed. Fig. 6 is another way to show the compensation force. The F_1 indicated by the dotted arrow shown in the Fig. 6 is the compensation force in the x-axis.

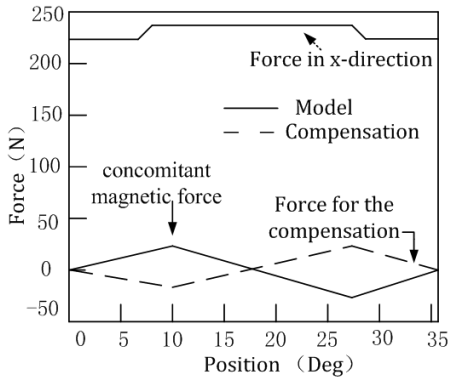

Fig. 5 The concomitant magnetic force and compensation force

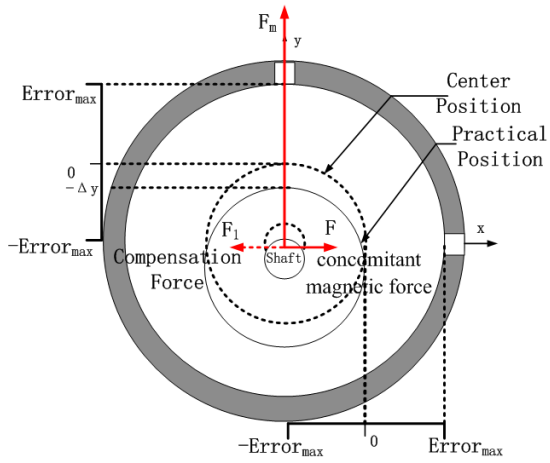

Fig. 6 Eccentric radial force of proposed motor

3.2 Mathematical model of the radial force

During the design, the mathematical model of the radial force has been defined, but that is a very complex mathematics. If this mathematical model was used, a higher efficient CPU is needed, and at the same time the ability of real time feedback is not as good as others, so it is not well for a higher preference control.

A approximate mathematical model was used for the realtime control. The mathematical model of radial force is as follows:

$$F = K_F i^2 \tag{1}$$

$$K_F = \mu_0 N^2 L_{stk} R \beta_r^3 / 2g^2 \tag{2}$$

Where μ_0 is the permeability of the air, N is the number of coil turns, L_{stk} is the motor stacking length, R is the rotor radius, β_r is one rotor pole arc, g is the air gap length, so the radial force the motor needed can be calculated by the air gap errors. Rotor radial displacements can be regulated with two independent close-loop air-gap displacement controllers, one for x- and the other for y-direction, respectively. These two PI controllers generate the desired radial force commands F_x^* and F_y^* as shown in following equations in order to keep the rotor position in the center.

$$F_x^* = K_p \cdot \Delta x + K_i \cdot dt \tag{3}$$

$$F_y^* = K_p \cdot \Delta y + K_i \cdot dt \tag{4}$$

In which K_p and K_i are the proportional and integral coefficient, respectively. The actual current values of selected radial force windings can be controlled through hysteresis method according to these two current command signals. The above control algorithms are realized using a TI TMS320F2812 DSP.

$$F_{cx} = f_{x1}(i_{x1} + \theta_{rm}) + f_{x2}(i_{x2} + \theta_{rm}) \tag{5}$$

$$F_{cy} = f_{y1}(i_{y1} + \theta) + f_{y2}(i_{y2} + \theta) \tag{6}$$

$$f_{x1} = f_{x1}LUT(x_k, y_k) \tag{7}$$

$$f_{x2} = f_{x2}LUT(x_k, y_k) \tag{8}$$

$$f_{y1} = f_{y1}LUT(x_k, y_k) \tag{9}$$

$$f_{y2} = f_{y2}LUT(x_k, y_k) \tag{10}$$

F_{cx} and F_{cy} are the compensation forces in the x- and y-direction. f_{x1}, f_{x2}, f_{y1} and f_{y2} are the lookup table values of the compensation force.

Fig. 7 shows the control block diagram of the BLSRM. Fig. 8 shows the block diagram of suspension control. In this diagram, the x and y are the displacement of the motor. The F_x and F_y is the command force. θ_{rm} is the rotor position. The i_1^*, i_2^*, i_3^* and i_4^* are the command current.

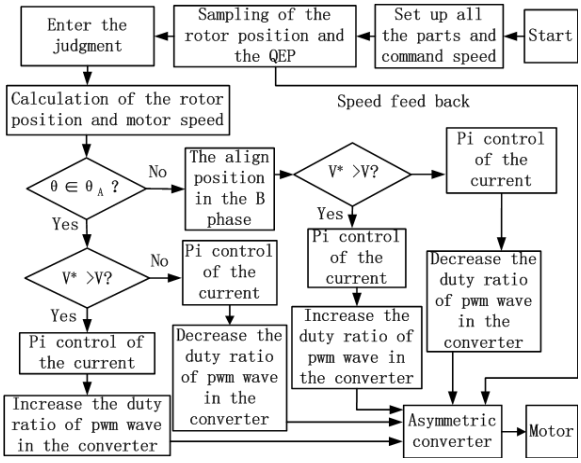

Fig. 7 Air-gap control system

The i_1^*, i_2^*, i_3^* and i_4^* are the real current. So the error in the air gap input to the PI controller, then the output is command force, by the current command block, the

output is the command current, combined with the real current to have the current directly control. Fig. 8 shows the detailed control block diagram of the current control. The PI control is used to meet the current error of the radial force current.

4. SIMULATION AND EXPERIMENTAL RESULTS

4.1 Control block diagram

Table 1 shows the specifications of the hybrid BLSRM. The rated power of this motor is 1kw. And maximum radial force is 200[N]. The maximum output torque is 0.8 N·m. Fig. 8 shows the control block diagram of the BLSRM. Combining with the Fig. 7, the x and y are the displacement of the motor. The F_x and F_y is the command force. θ_{rm} is the rotor position. The i_1^*, i_2^*,

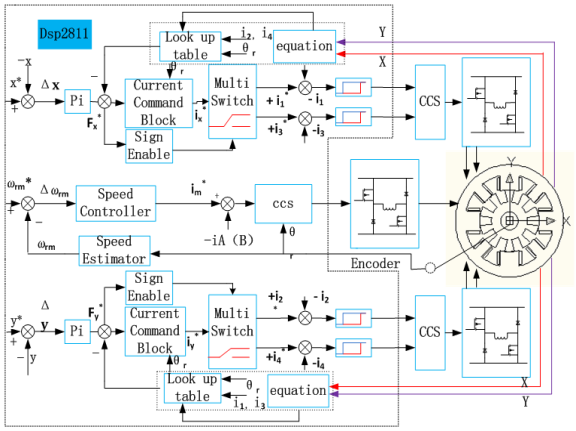

Fig. 8 Control block diagram

Table 1 Specifications of the prototype BLSRM

Parameter	Value
Number of Stator Poles	8
Number of Rotor Poles	10
Pole arc of stator for torque [deg]	18
Pole arc of stator for radial force [deg]	36
Pole arc of rotor [deg]	18
Length of axial stack [mm]	40
Outer Diameter of Stator [mm]	112
Inner Diameter of Stator [mm]	62
Yoke Thickness of Stator [mm]	10
Length of Air Gap [mm]	0.3
Shaft Diameter of Rotor [mm]	18
Yoke Thickness of Rotor [mm]	9.7

i_3^* and i_4^* are the command current. The i_1, i_2, i_3 and i_4 are the real current. So the error in the air gap input to the PI controller, then the output is command force, by the current command block, the output is the command current, combined with the real current to have the DCC (directly current control).

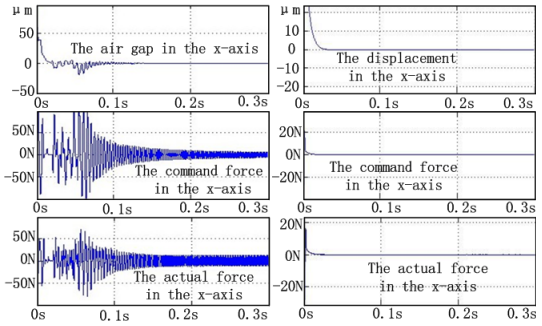

(a) Before compensation (b) After compensation

Fig. 9 Displacement of the rotor and radial force in the x-axis without and with compensation

4.2 Simulation results

Fig. 9(a) shows the displacement of the rotor and the radial force in the x-axis before compensation. The process of the operating of the motor is similar with last picture, but there aren't compensation parts in this control system. From the figure, there are many disturbances in the air gap, because the force in the radial force pole is unstable. It is not good for the operating of the bearingless SRM.

Fig. 9(b) shows the displacement of the rotor and the radial force in the x-axis after the compensation. The top picture shows the displacement in the x-direction, just the same as the air gap. The picture of the displacement is respect to the radial force in the next two pictures. The next two pictures show the command force and the real force in the x-direction. At first, the rotor is not in the center of the motor, so the radial force pole will generate the command force to keep the rotor in the center of the motor. Therefore there are some disturbance in the first step of the simulation. And then 0.03second later the air-gap keeps constant. It is the same condition in the y-axis, as showed in the Fig. 10.

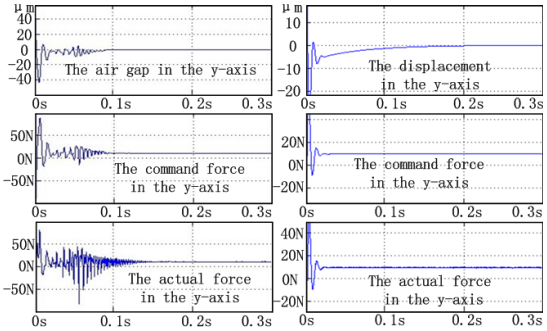

(a) Before compensation (b) After compensation

Fig. 10 The displacement of the rotor and the radial force in the y-axis before and after the compensation

Fig. 11 shows simulation result of the displacement of the rotor position before and after the compensation. The x-axis is the error of the air-gap in the x-direction, the y-axis is the error of the air-gap in the y-direction. The air-gap in the picture (a) is unstable. But after the compensation, the air-gap is uniform.

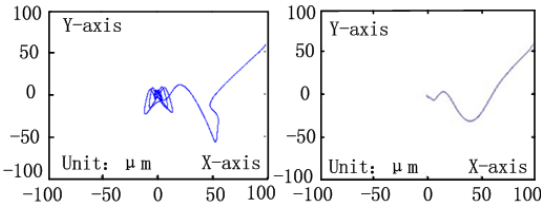

(a) before compensation (b) after compensation

Fig. 11 The simulation result of the displacement of the rotor position before and after the compensation

Fig. 12 shows radial force and currents in the suspending pole.

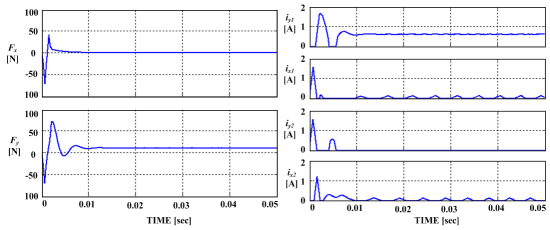

(a) radial force (b) Radial force currents

Fig. 12 the radial force and the currents in the suspending pole

Fig. 12(a) shows radial force in x- and y- direction and suspending winding currents. In order to bear the rotor in center position, the radial forces are controlled by the suspending winding currents regardless of motor speed and torque. In the simulation, 10 [N] loads is applied in rotor shaft at y-direction.

4.3 Experimental results

Fig. 13 shows the protype motor and the inverter. There are DSP board and the converter board including in this inverter.

Fig. 14 shows the air-gap displacements and winding currents when the motor speed is 2,500 [rpm]. The waveform of the torque winding current is same as conventional two-phases SRM. And the radial force winding currents are controlled to maintain the shaft position in the center. As shown in Fig. 14, the rotor stays in the center position during rotating.

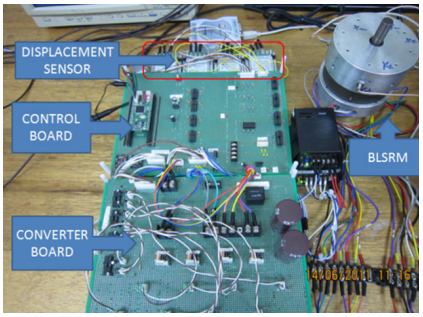

Fig. 13 Prototype BLSRM

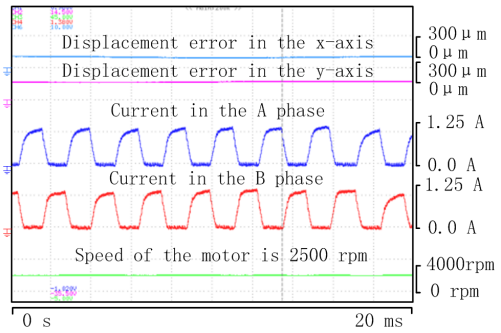

Fig. 14 Torque current and air gap displacement at the rotating condition with the speeds are 2500rpm

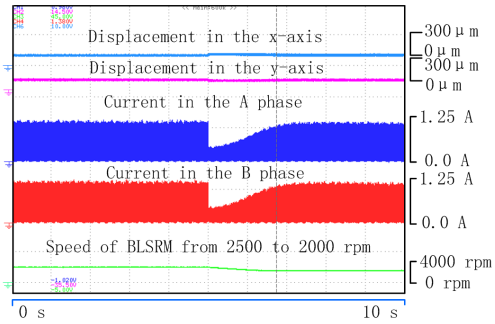

Fig. 15 Experiment result with speed variation (2500 to 2000 rpm)

In the Fig. 15, the motor speed is changed from 2,500 to 2,000[rpm]. According to speed changing, the torque winding current is changed to control the motor speed. But the air-gap displacements can keep the center position without any vibration. Fig. 16 shows displacements in both axis during the motor speed are changed from 2000 to 2500 rpm. And the condition of the wave form is similar with the Fig. 15.

Fig. 17 shows the experiment result when the speed is 4000 rpm. The upper 2 lines show the displacement value in the y- and x- axis, the third line from the top shows the speed of the motor. The 4th and 5th show the current in the torque pole. The 6th and last line show the current in the x- and y-axis.

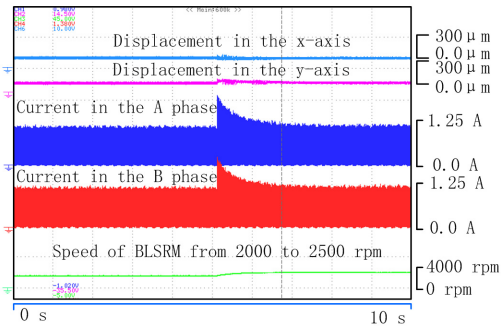

Fig. 16 Experiment result with speed variation 2000 to 2500 rpm)

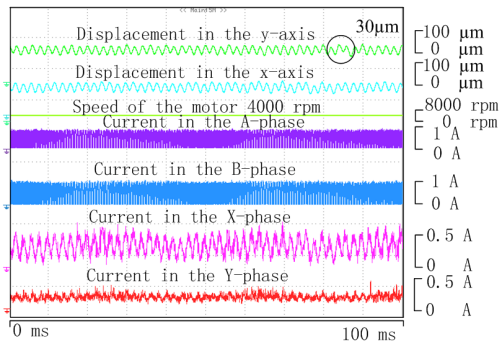

Fig. 17 Experimental result (4000rpm)

It can be seen that the current in the x-axis is much bigger than the y-axis, because of the precision of the motor manufacture. The air gap in the x-axis is a little bigger than the y-axis. So if the same radial force needed, a bigger current is generated in the x-axis. The current also varies with the air-gap, When there is a big air-gap in the x-axis, a current with an appropriate coefficient was generated in the -x axis. So in order to keep the rotor in the center of the motor, the coefficients in the x- and y-axis were different.

Fig. 18 shows the experiment result when the speed is and 6000 rpm. Different from the original, the speed is higher and the displacement error is bigger. At the same time the current is higher than before. The torque current is more smooth than before, and the effect of the manufacturing inequalities is more obvious than before.

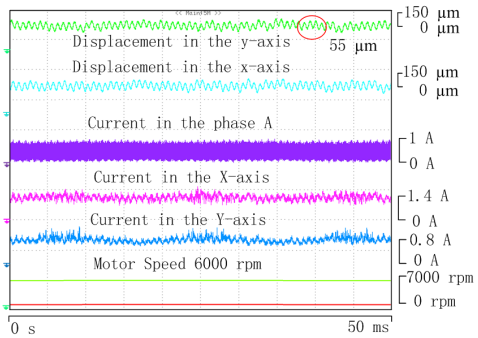

Fig. 18 Experimental result (6000rpm)

In the conventional control the maximum speed is 2000rpm, compared with the new control method the maximum speed rises to 8000rpm, and the accepted displacement error is 55 μm in 6000rpm.

Table 2 shows the comparition of the conventional control, current hysteresis control and DCC.

Table 2 Control performance comparison

	Conventional Control	Hysteresis Control	Current Directly Control
Maximum Speed	2000rpm	8000rpm	8000rpm
Displacement Error	50μm (2000rpm)	30μm (2000rpm)	25μm (2000rpm)
DisplacementError	None	30μm (3000rpm)	25μm (3000rpm)
DisplacementError	None	40μm (4000rpm)	30μm (4000rpm)
DisplacementError	None	60μm (5000rpm)	50μm (5000rpm)
DisplacementError	None	70μm (6000rpm)	55μm (6000rpm)
DisplacementError	None	90μm (8000rpm)	80μm (8000rpm)

5 CONCLUSION

This paper presents radial force control scheme of a 8/10 hybrid stator pole BLSRM. The each pole winding currents is concerned to torque and radial force production, respectively. For the real-time control, a compensation radial force control model is derived. Selection of radial force pole can be determined and corresponding currents can be calculated with the control model. The simulation results verified the validity of control strategy. Compared with conventional one, the proposed suspension control strategy is much more precise. The maximum speed can be reached 8000 rpm, And we can accept the displacement error at the 6000rpm. In the proposed BLSRM and control scheme, air-gap can be kept at the center position by the simulation and experimental results.

Acknowledgment

This work was supported by the National Research Foundation of Korea (NRF) grant funded the Korea Government(GrantNo.2010-0014172)

References

[1] F. Lin and S. Yang,"Self-bearing Control of a Switched Reluctance Motor Using Sinusoidal Currents," IEEE Trans. on Power Electronics, Nov. 2007: 2518-2526.

[2] W. Liu and S. Yang, "Modeling and Control of a Self-bearing Switched Reluctance Motor," in Proc 14th IAS Annual Meeting, Hong Kong, 2005: 2720-2725.
[3] Barnes M and Pollock C,"Power Electronic Converters for Switched Reluctance Drives," IEEE Trans. on Power Electronics, 1998, 13(6): 1100-1111.
[4] L.Chen and W.Hofman,"Performance Characteristics of One Novel Switched Reluctance Bearingless Motor Drive" in Power Conversion Conference 2007 (PCC'07), Nagoya, 2007:608-613.
[5] H. J. Wang, D. H. Lee and J. W. Ahn, "Novel Bearingless Switched Reluctance Motor with Hybrid Stator Poles: Concept, Analysis, Design and Experimental Verification," The Eleventh International Conference on Electrica Machines and Systems, 2008: 3358-3363.
[6] L.Chen and W.Hofman,"Performance Characteristics of One Novel Switched Reluctance BearinglessMotor Drive," in Power Conversion Conference 2007 (PCC '07), Nagoya, 2007:608-613.
[7] Carlos R.Morrison.Bearingless Switched Reluctance Motor. U.S. Patent 6,727,618, 2004
[8] Neil R.Garrigan, Wen L.Soong, Charles M.Stephens, et al,"Radial Force Characteristics of a Switched Reluctance Machine," IEEE Industry Applications Society Annual Meeting, Phoenix, Oct. 1999 : 2250-2258.
[9] Ye Shuang, Deng Zhiquanand Yan Yangguang, "New Formulae Based on Fourier Extension for Bearingless Switched Reluctance Motors," Proceedings of the 8th international symposium on magnetic bearings (ISMB-8), Mito, Japan, Aug. 26-28, 2002: 53-58.

저 자 소 개

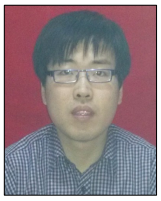

관 충 우 (關 忠 宇)

1986년생, 2009년 심양공업대 전기공정 및 자동화 공학과 졸업. 2012. 2 경성대 메카트로닉스공학과 석사. 현재 심양공업대 전기기기와 전기공학과 석사과정.
Tel : 051-663-4779
E-mail : guanzhongyu2525@163.com

안 진 우 (安 珍 雨)

1958년생. 1984년 부산대 전기공학과 졸업, 1992년 동 대학원 전기공학과 졸업 (박사), 1992년~현재 경성대 메카트로닉스공학과 교수. 현재 당학회 B부문 국제이사, Journal of International Conference on Electric Machines and Systems(JICEMS) 편집위원장, 지식경제부지정 고령친화 이지라이프 RIS 사업단장. 한국RIS협회장, Board Member of IEEE/IAS,
Tel : 051-663-4773,
E-mail : jwahn@ks.ac.kr